



# Silver nanoparticle-embedded pectin-based hydrogel for adsorptive removal of dyes and metal ions

Arun K. Kodoth<sup>1</sup> · Vishalakshi Badalamoole<sup>1</sup>

Received: 21 March 2018 / Revised: 20 February 2019 / Accepted: 25 March 2019 /

Published online: 3 April 2019

© Springer-Verlag GmbH Germany, part of Springer Nature 2019

## Abstract

Silver nanoparticles made by green synthesis have been incorporated into pectin-based copolymer gel to make a nanocomposite gel to be used as an adsorbent material for the removal of divalent metal ions and dyes from aqueous solutions. Silver nanoparticles were obtained by mixing silver nitrate with aqueous solution of pectin followed by microwave irradiation. The nanocomposite hydrogel was obtained by the microwave-assisted polymerization of 2-acrylamido-2-methyl-1-propane-sulfonic acid (AMPS) and acrylamide (AAm) in the presence of *N,N'*-methylenebis-acrylamide (MBA) in pectin solution containing silver particles. Characterization of the nanocomposite gel was done by FTIR, TGA, XRD, FESEM and EDS techniques. The system was evaluated for its capacity to adsorb cationic dye, crystal violet (CV) and metal ions [Cu(II) and Pb(II)] from aqueous solutions. The presence of Ag nanoparticles is observed to enhance the adsorption capacity of the gel for the above mentioned adsorbates. The kinetic studies revealed second-order adsorption processes which fit well into Langmuir model. The evaluation of thermodynamic parameters indicated the adsorption process to be exothermic and spontaneous. A maximum of 1950 mg/g CV, 111 mg/g Cu(II) and 130 mg/g Pb(II) could be removed from the aqueous solution which is quite high in comparison with other reported materials. The desorption studies indicated the possible reusability of the nanocomposite.

**Keywords** Nanocomposite hydrogel · Pectin · Silver nanoparticles · Microwave · Dye adsorption · Metal adsorption

✉ Vishalakshi Badalamoole  
vishalakshi2009@yahoo.com

<sup>1</sup> Department of Post-Graduate Studies and Research in Chemistry, Mangalore University, Mangalagangothri, DK, Karnataka 574199, India

## Introduction

Contamination of water bodies by industrial effluents is a serious environmental issue. Various techniques have been employed for the treatment of dye or metal ion contaminated water [1]. Water treatment by adsorption has received much attention due to the low cost involved, ease of separation of adsorbate, recyclability of the adsorbent and high efficiency of the method [2, 3]. Researchers have been interested in designing various adsorbent materials for water purification [4]. Nanocomposites [5], polymeric membranes [6], fruit peels [7], metal organic frameworks [8], polysaccharide-based nanocomposite hydrogels [9], interpenetrating networks [10] and semi-interpenetrating networks [11] are few among them. Among these adsorbents, polysaccharide-based hydrogels received much importance due to their unique capacity to hold large amount of contaminants within their network like structure [12]. Moreover, as polysaccharides are derived from microorganisms or plants, they have the additional advantages of being non-toxic and biodegradable [13].

Hydrogels are polymeric materials which are capable of holding water molecules through the process called swelling [14]. They are three dimensional networks of polymer chains which can swell but not dissolve in water. They are composed of natural or synthetic materials possessing high degree of flexibility. The structural variations and alteration in water holding capacity of hydrogel network can be obtained by varying the nature of the polymer, degree of cross-linking, etc. Indeed, many novel hydrogels of synthetic or natural polymers with a plethora of aims were synthesized and tested in different fields [15–17].

There are several reports available in the literature on adsorbent materials based on modified polysaccharide hydrogels for use in water purification. Modifications have been achieved by graft polymerization with synthetic monomers [17] or by incorporation of nanoparticles of metals and metal oxides [18, 19]. Kono [20] reported the preparation of a range of amphoteric cellulose hydrogels for the adsorptive removal of three different anionic dyes. Graft copolymer of gellan gum and poly(DMAEMA) is used for the adsorptive removal of methyl orange from aqueous solutions [21]. High efficiency has been achieved for methylene blue removal by superabsorbent cellulose clay nanocomposite which also exhibited high mechanical strength [22]. A nanosilica containing xanthan gum-graft-polyacrylamide exhibited high adsorption toward methylene blue and methyl violet [23]. An adsorbent system of chitosan, AMPS and laponite has been described for the removal of Cu(II) from aqueous solution [3]. It is evident from the above studies that the presence of nanoparticles makes the hydrogels good adsorbents for dye molecules and metal ions.

In our earlier work [24], we have reported the synthesis of a new polysaccharide-based gel system consisting of gellan gum, PVA and acrylamide which has exhibited good adsorption capacity and usefulness for removal of crystal violet from aqueous solutions.

Based on the extensive literature on the use of graft copolymers and nanocomposites of polysaccharides for the adsorption processes, it was decided to develop

a new polysaccharide-based adsorbent material that can be effectively used for the removal of both dye molecules and metal ions from aqueous solutions. Pectin (Pec) is an anionic polysaccharide that is present in all citrus plants. It is mainly obtained from the citrus fruit peel extract and widely used in the food industry [25]. The hydrogels derived from Pec find a variety of applications as adsorbent materials for water purification [26], as drug delivery devices [27], as biomedical implants [28] and as food packaging materials [29]. Poor mechanical strength has always been a disadvantage of the polysaccharide-based hydrogels which is also found in pectin hydrogels [30].

The widespread applications of the silver nanoparticles (AgNPs) in diverse fields have been well established. The literature expounded the use of these nanoparticles as adsorbent materials for dyes and metal ions [31]. Hence, we have attempted to make a novel pectin-graft-copolymer gel with silver nanoparticles embedded in it. A detailed study of evaluation of the hybrid gel made as adsorbent material for removal of organic dyes and metal ions has been reported using the cationic dye, crystal violet and divalent metal ions: Cu(II) and Pb(II) from aqueous solutions.

## Materials and methods

### Materials

Analytical reagent grade chemicals were used throughout the experiments. Pectin (Pec), 2-acrylamido-2-methyl-1-propanesulfonic acid (AMPS) and lead chloride were obtained from Sigma-Aldrich Co., Germany. Acrylamide (AAm) was obtained from Loba Chemie, India. *N,N'*-Methylene-bis-acrylamide (MBA), ammonium peroxydisulfate (APS), copper sulfate and methanol were obtained from Spectrochem Pvt. Ltd., Mumbai, India. Silver nitrate was obtained from NICE Chemicals (P) Ltd., Kochi, India. Crystal violet (CV) with a purity of 96.0% was obtained from Rankem, RFCL Ltd., Delhi, India. Double distilled water was used in all the experiments.

### Methods

#### Microwave-assisted formation of silver nanoparticles (AgNPs) in the presence of Pec

To 20.0 mL of 0.5% aqueous solution of Pec, 10.0 mL of aqueous silver nitrate solution (0.018 mmol) was added and irradiated with microwave for 1 min at a power of 80 W. The deep brown solution containing AgNPs along with Pec was used for the preparation of the nanocomposite hydrogel.

## Microwave-assisted synthesis of pectin-graft-(poly(2-acrylamido-2-methyl-1-propanesulfonic acid)-polyacrylamide)/Ag nanocomposite hydrogel [Pec-*g*-poly(AMPS-*co*-AAm)/Ag]

To the solution containing Pec and AgNPs, 0.15 g (0.724 mmol) AMPS and 0.4 g (5.627 mmol) AAm were added and stirred, using a magnetic stirrer for 24 h. To this well-stirred mixture, 1.0 mL (0.066 mmol) of aqueous APS was added and stirring continued for 1 h which was followed by the addition of 3.0 mL (0.292 mmol) aqueous MBA. The solution was maintained under stirring for 3 h and later irradiated with microwave of 80 W power for 30 s. The resultant gel was then kept immersed in methanol overnight to remove the unreacted monomers and dried in a hot air oven for 24 h at 50 °C. Pec-*g*-poly(AMPS-*co*-AAm) hydrogel was made using 20.0 mL of 0.5% aqueous solution of Pec directly and following the above procedure.

### Characterization techniques

#### Fourier transform infrared (FTIR) spectroscopy

FTIR spectra of Pec-*g*-poly(AMPS-*co*-AAm) and Pec-*g*-poly(AMPS-*co*-AAm)/Ag were recorded on a Shimadzu IR Prestige 21 (Japan) FTIR spectrophotometer in transmittance mode in the range of 500–4000 cm<sup>-1</sup>.

#### Field emission scanning electron microscopy (FESEM) and energy-dispersive X-ray spectroscopy (EDS)

Morphological study of Pec-*g*-poly(AMPS-*co*-AAm) and Pec-*g*-poly(AMPS-*co*-AAm)/Ag samples were carried out by recording the FESEM images using JEOL-JSM5800LV (Japan) Scanning electron microscope. The micrographs were recorded with different magnifications under a voltage of 3.0 kV. Using the same instrument, the energy-dispersive X-ray spectrum of both the samples was recorded and the amount of different elements in each sample was analyzed.

#### X-ray diffraction (XRD)

Benchtop X-ray diffractometer, Rigaku MiniFlex 600 (Japan), was used to record the powder X-ray pattern of Pec-*g*-poly(AMPS-*co*-AAm) and Pec-*g*-poly(AMPS-*co*-AAm)/Ag. The diffraction patterns were recorded in the angle range of 10° to 80° at 30 °C at the recording rate of 2°/min.

#### Thermogravimetric analysis (TGA)

Thermal decomposition patterns of Pec-*g*-poly(AMPS-*co*-AAm) and Pec-*g*-poly(AMPS-*co*-AAm)/Ag were obtained using thermogravimetric analyzer SDT

Q600 V20.9 (Japan). The samples were heated from room temperature to 700 °C under nitrogen atmosphere at a rate of 10 °C/min.

### Transmission electron microscopy (TEM)

TEM images of the nanocomposite were recorded by JEOL/JEM 2100 transmission electron microscope (USA) operating at 200 kV.

### Swelling studies

Equilibrium swelling measurements of the samples have been carried out in double distilled water (pH 7.0) and in aqueous buffer solutions of varying pH (1.2, 3.0, 9.0 and 13.0). Pre-weighed dry samples of Pec-*g*-poly(AMPS-*co*-AAm) and Pec-*g*-poly(AMPS-*co*-AAm)/Ag were kept immersed in 50 mL of the swelling medium contained in a beaker at room temperature. After specific intervals of time, the swollen gels were taken out; the surface-adhered liquid droplets were removed by blotting with filter paper and weighed using SHIMADZU AUX 120 (Japan) Electronic Balance with an accuracy of  $\pm 0.1$  mg. The increase in weight was recorded. The weight measurements were taken till equilibrium is attained indicated by the constant weight of the swollen sample. The swelling ratio, SR (g/g) at a given time, is calculated using the equation:

$$SR = \frac{W_t - W_0}{W_0} \quad (1)$$

where  $W_t$  is the weight of the swollen gel and  $W_0$  is that of the dry gel.

### Adsorption studies

#### Dye and metal adsorption studies

Dye and divalent metal adsorption studies were carried out by batch process in deionized water using CV as model dye; Cu(II) and Pb(II) as model metal ions using the following procedure. A mass of 20 mg of nanocomposite samples was suspended in dye and metal salt solutions of concentrations varying from 20–2000 ppm and 10–200 ppm, respectively. The samples were found to saturate after 7 h when kept immersed in dye solution, whereas it took only 2 h for the saturation with metal ions. Therefore, the samples were allowed to equilibrate for 7 h in the case of dye and 2 h in the case of metal ions, respectively, at 28 °C. The amount of unadsorbed dye was calculated from the absorbance of the decanted dye solution using UV–Vis spectrophotometer (Shimadzu UV-160A, Japan) at the wavelength of 588 nm, and the concentration of the metal ions in the supernatant solution was determined using GBC 932 Plus Atomic Absorption Spectrophotometer (Australia). The equilibrium dye or metal ion adsorption capacity,  $Q_e$  (mg/g), of the nanocomposite was calculated using the following equation:

$$Q_e = (C_i - C_e) \times \frac{V}{m} \quad (2)$$

where  $C_i$  is the initial concentration of dye/metal ion (mg/L),  $C_e$  is the residual concentration of dye/metal ion at equilibrium (mg/L),  $V$  is the volume of solution (L), and  $m$  is the amount of dry Pec-*g*-poly(AMPS-*co*-AAm)/Ag (mg) used for the adsorption studies.

### Desorption studies

Desorption experiments were carried out to check the reusability of the gel and the nanocomposite for removal of dye/metal ions. About 20.0 mg each of the polymer samples was suspended in separate dye and metal salt solutions of initial concentrations of 25 mg/L. The samples loaded with adsorbate were separated by centrifugation, washed with water and dried. About 20.0 mg of the dry samples was suspended in 20.0 mL of stripping solution of pH 1.2 (prepared using HCl solution). The solutions were stirred for 2 h at 28 °C and centrifuged. The concentration of the dye and metal ions in the supernatant was determined using UV–Vis spectrophotometer and AAS, respectively. The percentage of desorption ( $D$ ) was calculated using the following equation:

$$D(\%) = \frac{\text{Amount of dye molecules/metal ions desorbed}}{\text{Amount dye molecules/metal ions adsorbed}} \times 100 \quad (3)$$

### Leaching of AgNPs

The Ag nanoparticles are likely to diffuse out of the swollen gel upon contact with the swelling medium. To check and quantify this, the nanocomposite was suspended in double distilled water for a total duration of 24 h. The supernatant liquid was analyzed by dynamic light scattering technique using the instrument Nano ZetaSizer (Malvern Instruments, Malvern, UK) where the percentage of particle counts rate (kcps) was obtained.

## Results and discussion

### Synthesis of Pec-Ag nanocomposite

The polysaccharide Pec functions both as a capping agent and a stabilizing agent, while microwave irradiation helps to reduce the  $\text{Ag}^+$  to  $\text{Ag}^0$  in the presence of the polysaccharide. On passing microwave, the homogenous solution becomes yellow in color which on continuous irradiation results in dark brown solution indicating the formation of silver nanoparticles [32, 33].

### Microwave-assisted synthesis of Pec-*g*-(PAMPS-*co*-PAAm)/Ag

Microwave irradiation of the polymerization mixture containing APS results in the formation of free radicals from the APS initiator. The sulfate radicals extract H from –OH group on Pec-generating macroradicals which act as site for grafting

of poly(AMPS-*co*-AAm) chains. The presence of MBA leads to the cross-linking of graft copolymer and enhances the mechanical stability of the gel. When the gel is made with Pec solution containing AgNPs, the nanoparticles get incorporated into the network, occupying the free space between the chain segments. The hydrogel prevents the aggregation of silver nanoparticles within the system. The mechanism of formation of [Pec-*g*-poly(AMPS-*co*-AAm)/Ag] nanocomposite is shown in Fig. 1.

### Characterization

#### FTIR spectroscopy

Figure 2a illustrates the FTIR spectrum of Pec-*g*-poly(AMPS-*co*-AAm). Bands in the range 3250–3500  $\text{cm}^{-1}$  are due to the –OH and NH stretching vibrations of pectin and AAm, respectively. The –C–H stretching vibration is observed at 2920  $\text{cm}^{-1}$ . The C=O stretching of pectin is observed at 1685  $\text{cm}^{-1}$ . The absorption band at 1588  $\text{cm}^{-1}$  is attributed to the stretching frequency of the –COOH group of pectin. The bands around 1416 and 1322  $\text{cm}^{-1}$  are due to –CH<sub>2</sub> scissoring and –OH

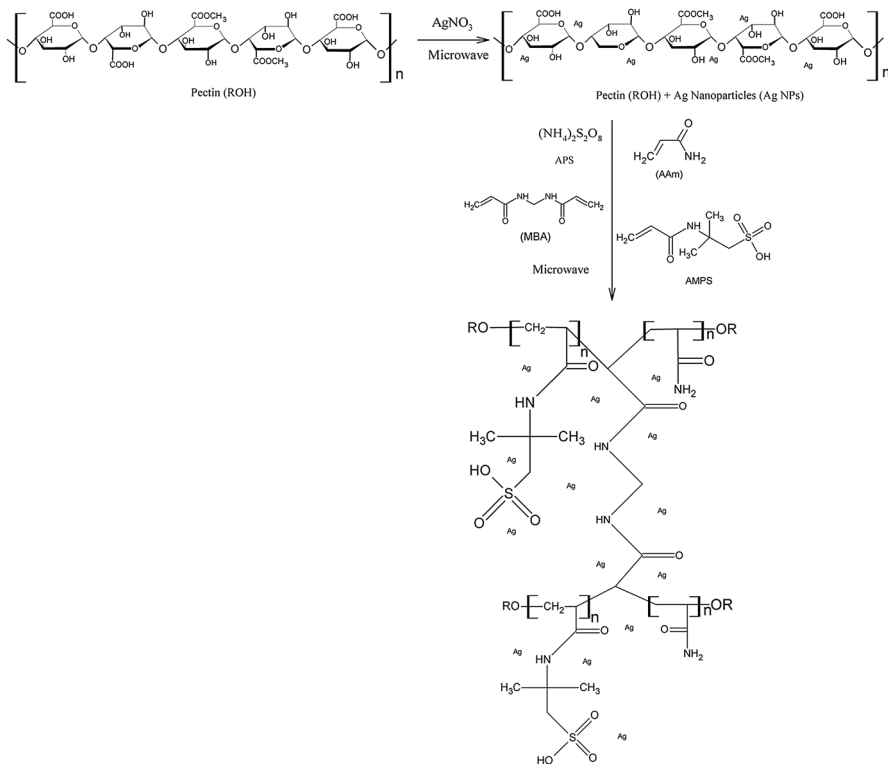
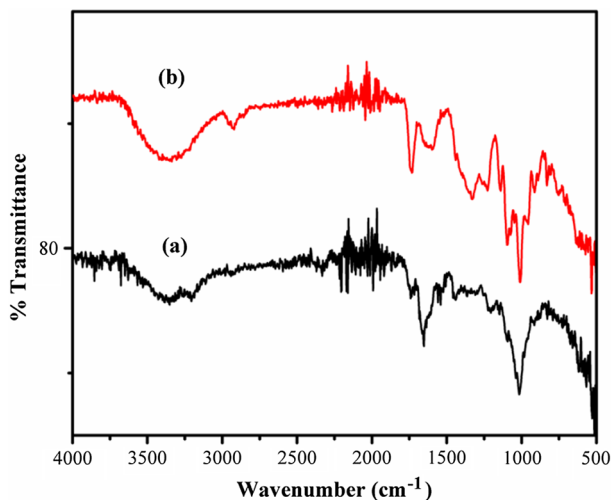


Fig. 1 Mechanism of formation of Pec-*g*-poly(AMPS-*co*-AAm)/Ag nanocomposite



**Fig. 2** FTIR spectrum of (a) Pec-*g*-poly(AMPS-*co*-AAm) and (b) Pec-*g*-poly(AMPS-*co*-AAm)/Ag

bending vibrations, respectively. The S=O stretching of AMPS occurs at  $1040\text{ cm}^{-1}$  [34]. The band at  $1019\text{ cm}^{-1}$  is due to  $-\text{C}-\text{O}-\text{C}$  stretching of Pec. The FTIR spectrum of Pec-*g*-poly(AMPS-*co*-AAm)/Ag is shown in Fig. 2b. Significant changes have been observed in the spectrum of the nanocomposite due to the interaction of silver nanoparticles with the polysaccharides backbone. The additional band due to the interaction of silver nanoparticles ( $\text{O}-\text{Ag}-\text{O}$ ) with the hydroxyl and carboxyl groups of pectin arises at  $626\text{ cm}^{-1}$  [35].

### FESEM and EDS analyses

Surface morphological features of the parent gel, Pec-*g*-poly(AMPS-*co*-AAm), and its silver nanocomposite, Pec-*g*-poly(AMPS-*co*-AAm)/Ag, are shown in Fig. 3. The rough, layered morphology of the Pec-*g*-poly(AMPS-*co*-AAm) gel surface with few folding and voids has been changed to plane surface with uniform distribution of silver nanoparticles throughout the surface in the nanocomposite sample. Energy-dispersive spectra of the gel and the nanocomposite have been recorded to confirm the presence of AgNPs within the system and are shown in Fig. 3c, d. The amount of Ag in the nanocomposite is found to be about 4% of the total weight of the sample.

### XRD analysis

X-ray diffraction pattern of the Pec-*g*-poly(AMPS-*co*-AAm) gel shows a broad band indicative of amorphous nature of the system (Fig. 4a). The incorporation of silver nanoparticles imparts crystallinity to the nanocomposite. The intense sharp peaks observed in Fig. 4b are indicative of the presence of AgNPs which are embedded within the composite system. The major peaks due to AgNPs are found at  $2\theta$  angles



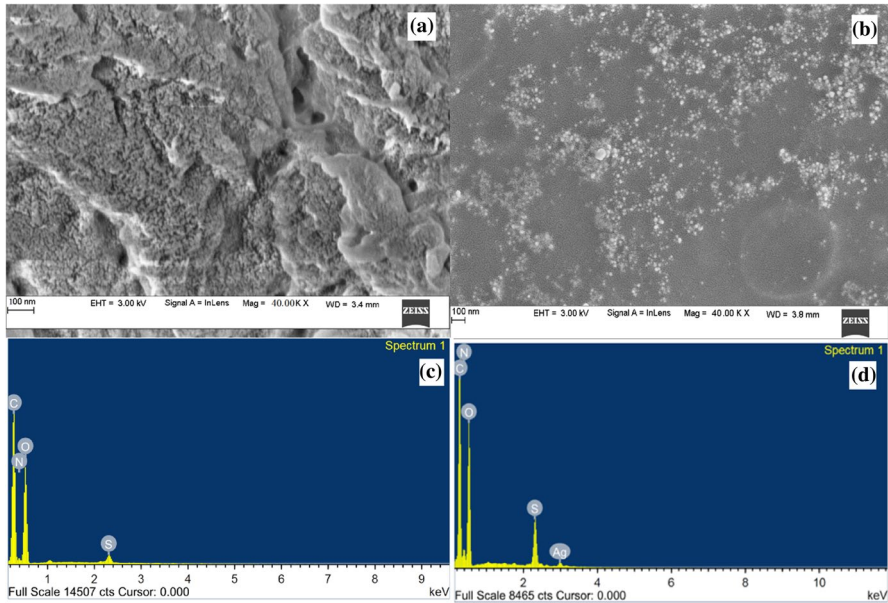


**Fig. 3** FESEM images of **a** Pec-g-poly(AMPS-co-AAm) and **b** Pec-g-poly(AMPS-co-AAm)/Ag; EDS spectra of **c** Pec-g-poly(AMPS-co-AAm) and **d** Pec-g-poly(AMPS-co-AAm)/Ag

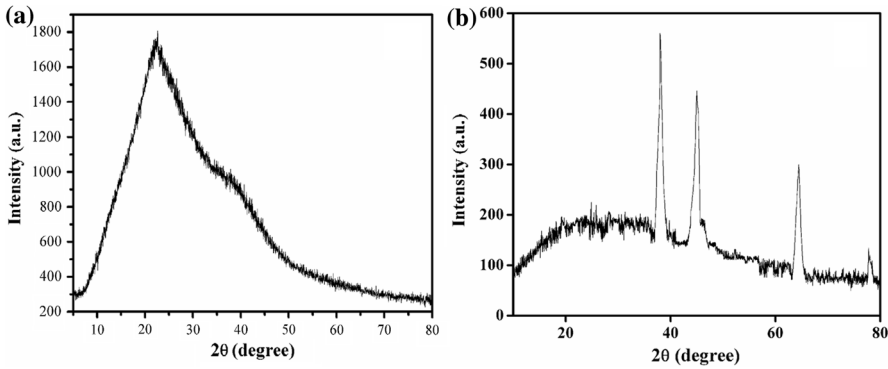


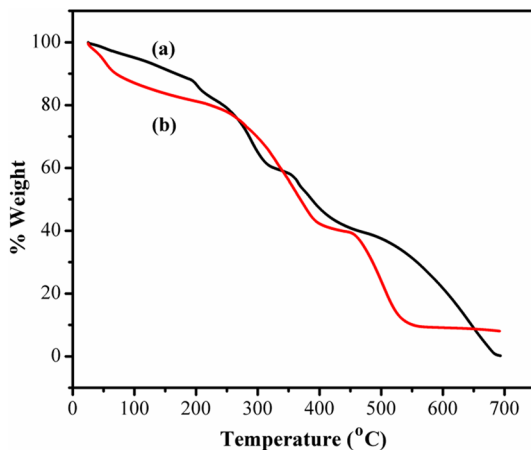
**Fig. 4** X-ray diffractograms of **a** Pec-g-poly(AMPS-co-AAm) and **b** Pec-g-poly(AMPS-co-AAm)/Ag

of 38°, 45°, 64.44° and 77.8° indicating the FCC structure which is in agreement with the literature reports [36].

**TGA analysis**

The thermograms of (a) Pec-g-poly(AMPS-co-AAm) and (b) Pec-g-poly(AMPS-co-AAm)/Ag are shown in Fig. 5. The parent system (Fig. 5a) shows a three-stage thermal degradation. The first stage of degradation is attributed to the loss

**Fig. 5** Thermograms of (a) Pec-g-poly(AMPS-co-AAm) and (b) Pec-g-poly(AMPS-co-AAm)/Ag



of water from the gel which is between room temperature and 100 °C. The second step of degradation is between 240 and 310 °C, due to the elimination of smaller molecules such as carbon monoxide and carbon dioxide. The third and final stage of degradation begins at a temperature 370 °C and gradually proceeds until complete degradation of the hydrogel at 670 °C due to degradation of the polysaccharide backbone. A slight difference in the degradation pattern is observed in the case of nanocomposite hydrogel (Fig. 5b). Here, the first stage of degradation begins at room temperature and lasts up to 100 °C, attributed to water loss. The higher amount of water loss in the case of nanocomposite is due to the hydrophilic nature of the AgNPs. The second stage of the degradation process is between 250 and 380 °C which occurs due to the degradation of the polysaccharide chain by eliminating carbon monoxide and carbon dioxide molecules. The final stage of degradation process occurs at 460–525 °C, resulting in degradation of the side chains leaving behind 8% of residual mass which is attributed partly to Ag particles. No further change in weight of nanocomposite is observed upon further heating.

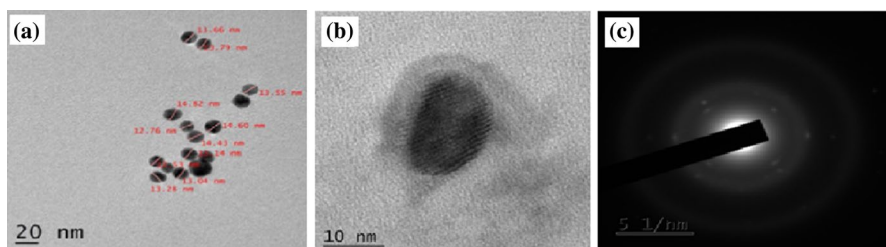


**Fig. 6** **a** TEM image of Pec-g-poly(AMPS-co-AAm)/Ag; **b** enlarged image of single AgNP and **c** SAED pattern of Pec-g-poly(AMPS-co-AAm)/Ag

### TEM analysis

TEM images of the AgNPs along with the selected area electron diffraction (SAED) pattern are given in Fig. 6. A high dispersion of AgNPs with size ranging from 12.7 to 14.5 nm (Fig. 6a) has been observed. The enlarged portion of the nanoparticles (Fig. 6b) confirms the spherical nature. The SAED pattern (Fig. 6c) shows three diffraction rings. The bright inner ring closest to the center is attributed to the combination of the (111) and (200) reflections, while the second ring corresponds to (220) plane. Further, the weakest outermost ring is due to (420) or (422) reflections [37].

### Swelling studies

The swelling behavior of the gel Pec-g-poly(AMPS-co-AAm)/Ag under different pH conditions is shown in Fig. 7. In addition to the extent of cross-linking, the swelling of the hydrogel system is mainly influenced by the hydroxyl and carboxyl groups of Pec; sulfonate group of AMPS; amide groups of MBA and AAm. As the pH was changed from 1.2 to 7, the equilibrium swelling increased, and with further change from neutral to basic range, the equilibrium swelling decreased drastically. The presence of large number of ionizable groups makes the polymer exhibit pH-dependent swelling. As the pH of the medium increases above the pKa of Pec (3.5), a drastic increase in swelling is observed. At pH lower than pKa value of Pec, the carboxylic groups of Pec are in undissociated state and the gel exhibits low swelling. As the pH increases above the pKa value, the swelling ratio increases [38]. The sulfonic groups of AMPS ionize fairly easily at all pH. This aids in attracting the polar water molecules to the sulfonate ions, resulting in the high water absorption capacity of the hydrogel. The acrylamide units being non-ionic do not affect swelling [39]. Moreover, the hydrogen bonding of water molecules with the functional groups of the network also contributes to the increased swelling in neutral pH. In basic medium,

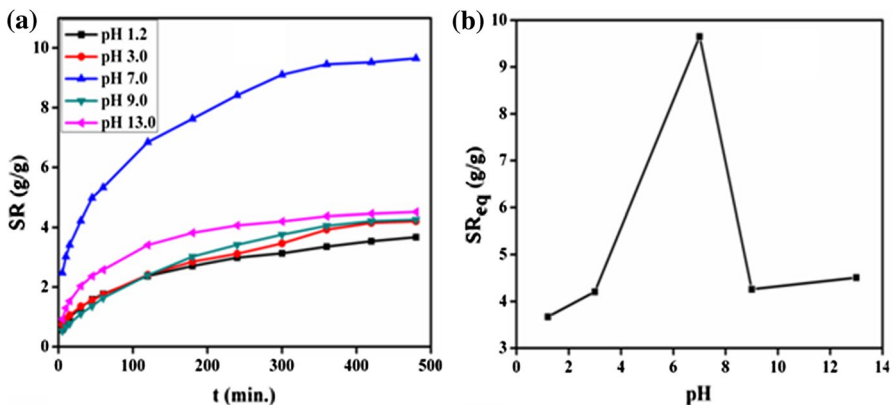
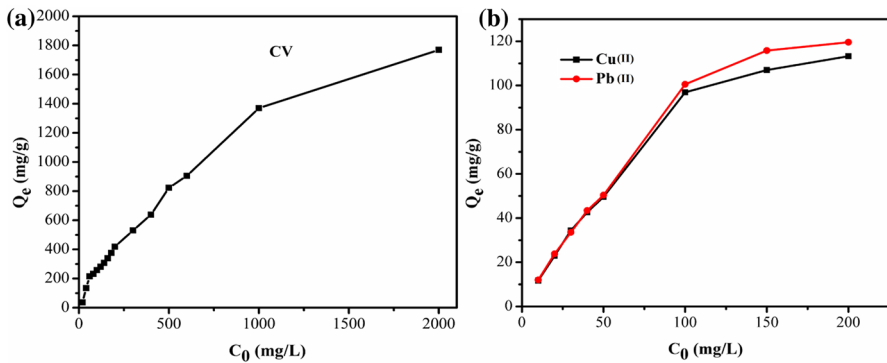
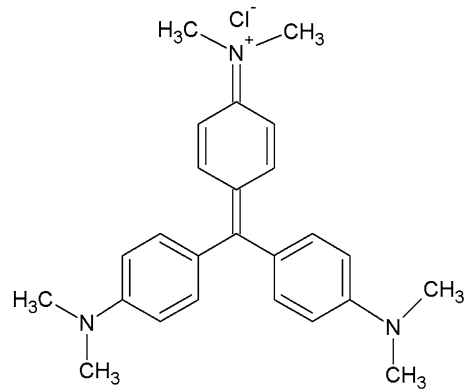


Fig. 7 a Dynamic swelling data and b equilibrium swelling data for Pec-g-poly(AMPS-co-AAm)/Ag under varying pH conditions

**Fig. 8** Structure of crystal violet**Fig. 9** The effect of initial concentrations of dye and metal ions on adsorption for Pec-g-poly(AMPS-co-AAm)/Ag. C V: contact time: 7 h, volume: 50 mL, pH: 7.0. Cu(II) and Pb(II): contact time: 2 h, volume: 25 mL, pH: 7.0

screening of charges on the network by electrolytes present in the medium results in the contraction of gel network and the swelling ratio decreases again.

### Adsorption studies

CV is a cationic dye with the molecular formula  $C_{25}N_3H_{30}Cl$  whose structure is shown in Fig. 8. Adsorption experiments were carried out in deionized water with varying concentrations of CV, Cu(II) and Pb(II), keeping all other parameters constant. Kinetic and isotherm studies of adsorptions were carried out at room temperature.

#### Effect of initial dye/metal ion concentration

The effect of initial adsorbate concentration on adsorption process for the sample Pec-g-poly(AMPS-co-AAm)/Ag is displayed in Fig. 9. The extent of adsorption is found to increase as the dye concentration increases and attains a constant value

around 2000 mg/L dye concentration and 200 mg/L metal concentration. Pectin is rich with functional groups such as carboxylic acid and hydroxyl groups which help in binding of cationic dye molecules and metal ions [1]. In deionized water, the carboxylic acid groups are in deprotonated state and act as sites for binding with cationic species. The sulfonate groups present at the PAMPS chain provides additional binding reactive sites for the cationic species by electrostatic interaction. The primary amine groups of PAAM bind to metal ions via coordinate bonds. In addition to this, metal ions form coordinate bond with the oxygen atoms of carbonyl and sulfonate groups of the system. Together with these reactive sites, the surface of Ag nanoparticles can provide sites where the dye molecules accumulate, thereby enhancing the adsorption process.

**Adsorption isotherm studies** The adsorption data obtained have been fit into three types of adsorption isotherm models: the Freundlich [40], Langmuir [41] and Temkin [42] models.

The mathematical expression of Freundlich isotherm is as follows:

$$Q_e = K_F C_e^{1/n} \tag{4}$$

The logarithmic form of above equation is

$$\log Q_e = \log K_F + \frac{1}{n} \log C_e \tag{5}$$

where ‘ $Q_e$ ’ is the amount of dye adsorbed per unit mass of adsorbent at equilibrium (mg/g), ‘ $C_e$ ’ is the concentration of the dye solution at equilibrium (mg/L), and ‘ $K_F$ ’ and ‘ $n$ ’ indicate the extent of the adsorption and the degree of nonlinearity between the solution concentration and the adsorbate, respectively, and are known as Freundlich adsorption isotherm constants. The intercept and slope of the plot between ‘ $\log Q_e$ ’ and ‘ $\log C_e$ ’ gives the values of  $K_F$  and  $n$ . Adsorption process can be considered as favorable only if the value of  $n$  lies between 1 and 10.

As per Langmuir model, a monolayer formation occurs at the surface of the adsorbent at the equilibrium stage. The equation representing Langmuir adsorption isotherm is expressed as:

$$\frac{C_e}{Q_e} = \frac{1}{Q_m} C_e + \frac{1}{Q_m K_L} \tag{6}$$

where ‘ $C_e$ ’ and ‘ $Q_e$ ’ are as defined earlier, ‘ $Q_m$ ’ is the maximum amount of adsorbate getting adsorbed on the surface of adsorbent (mg/g), and ‘ $K_L$  (l/mg)’ is the Langmuir constant.  $R_L$ , the separation factor, is the essential characteristics of the Langmuir isotherm, which is calculated as per the equation,

$$R_L = \frac{1}{1 + K_L C_0} \tag{7}$$

where  $C_0$  (mg/L) is the initial concentration of adsorbent corresponding to maximum adsorption.

The adsorbent–adsorbate interactions can be explained by Temkin isotherm model as well. It is based on the assumption that the heat of adsorption of all molecules would decrease linearly. The model is mathematically expressed as given in Eq. 8. The constants of Temkin isotherm model were calculated from the intercept and slope of the plot of ' $Q_e$ ' versus ' $\ln C_e$ '.

$$Q_e = \frac{RT}{b_T} \ln(A_T C_e) \quad (8)$$

where  $Q_e$  and  $C_e$  are as defined earlier.  $R$  is universal gas constant (8.314 J/mol/K);  $b_T$  is Temkin isotherm constant;  $A_T$  is Temkin isotherm equilibrium bridging constant (L/g); and  $T$  is the temperature in Kelvin.

The value  $\frac{RT}{b_T}$  is a constant which is related to heat of sorption and is represented by  $B$ .

The adsorption data obtained were plotted as per Eqs. (5), (6) and (8) and are shown in Fig. 10. The values of the constants  $K_L$ ,  $Q_m$ ,  $K_F$ ,  $n$ ,  $A_T$ ,  $b_T$  and  $B$  were determined from the intercepts, and slopes of their respective linear plots are presented in Table 1.

The obtained  $R_L$  values for the adsorption of both the metal ions and the dye lie in between 0 and 1 which indicates the favorable adsorption process at the specified

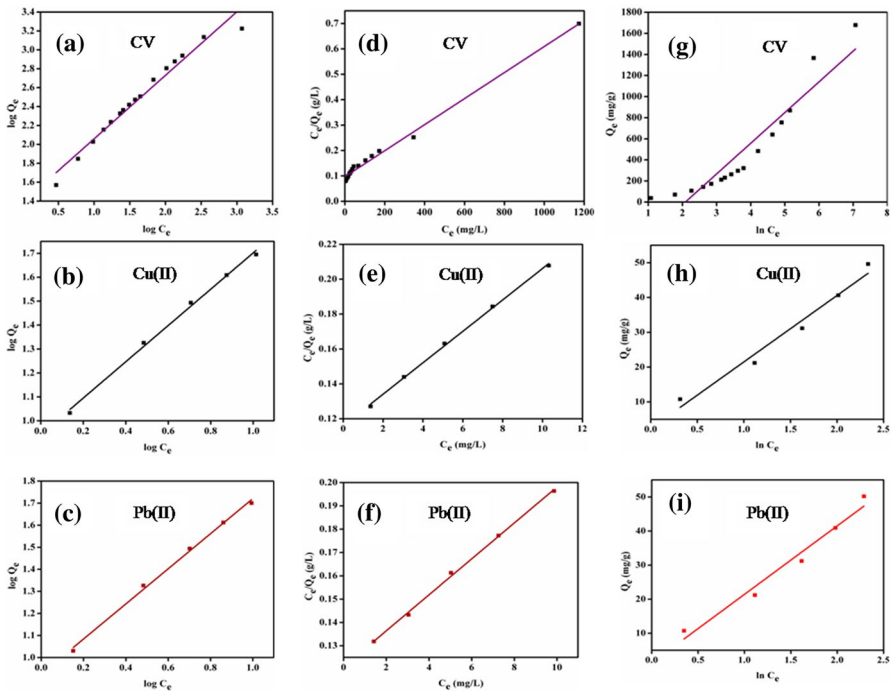


**Fig. 10** a–c Freundlich; d–f Langmuir; g–i: Temkin plots for the adsorption of CV, Cu(II) and Pb(II) on Pec-g-poly(AMPS-co-AAm)/Ag

**Table 1** Freundlich and Langmuir adsorption parameters for the adsorption of CV, Cu(II) and Pb(II) on Pec-g-poly(AMPS-co-AAm)/Ag

Isotherm models	Parameters	Adsorbate		
		CV	Cu(II)	Pb(II)
Freundlich	$K_F$	24.34	8.78	8.42
	$n$	1.49	1.32	1.26
	$R^2$	0.970	0.996	0.997
Langmuir	$R_L$	0.0862	0.2049	0.2387
	$K_L$	0.0053	0.0776	0.0638
	$Q_m$ (mg/g)	1950	111	130
	$R^2$	0.993	0.998	0.998
Temkin	$B$	291.46	19.09	20.10
	$A_T$	0.12	1.13	1.07
	$b_T$	8.50	129.80	123.26
	$R^2$	0.878	0.966	0.963

conditions. The highest value of  $R^2$  is obtained for Langmuir fit among the three isotherm models. The maximum adsorption capacity of Pec-g-poly(AMPS-co-AAm)/Ag is found to be 1950 mg for CV, 111 mg for Cu(II) and 130 mg for Pb(II), per gram of adsorbent.

**Adsorption kinetic studies** The kinetic analysis of adsorption data collected as a function of time has been made using two models, namely the Lagergren ‘pseudo-first-order model’ [41] and the Ho ‘pseudo-second-order model’ [43].

*The Lagergren ‘pseudo-first-order model’*

It is based on the assumption that the rate of change of adsorbate uptake over time is directly proportional to the difference in saturation concentration and the amount of adsorbate uptake over time. The mathematical representation of pseudo-first-order model is as follows:

$$\frac{dQ_t}{dt} = k_1(Q_e - Q_t) \tag{9}$$

where  $Q_e$  is the amount of adsorbate adsorbed at equilibrium (mg/g),  $Q_t$  is the amount of adsorbate adsorbed per unit of adsorbent (mg/g) at time  $t$ ,  $k_1$  is the pseudo-first-order rate constant ( $\text{min}^{-1}$ ), and  $t$  is the contact time (min).

Integrating the above equation and noting that  $Q_t=0$  when  $t=0$

$$\log(Q_e - Q_t) = \log Q_t - \frac{k_1 t}{2.303} \tag{10}$$

The  $Q_e$  and  $k_1$  values are calculated from the intercept and slope of the plot of  $\log(Q_e - Q_t)$  versus  $t$ .

*The Ho ‘pseudo-second-order model’*

The Ho ‘pseudo-second-order’ can be represented by the equation

$$\frac{dQ_t}{dt} = k_1(Q_e - Q_t)^2 \tag{11}$$

On integrating the above equation with boundary conditions,  $Q_i=0$  at  $t=0$ , we get,

$$\frac{t}{Q_i} = \frac{1}{k_2 Q_e^2} + \frac{t}{Q_e} \quad (12)$$

where  $k_2$  is the pseudo-second-order rate constant (g/mg/min). The initial adsorption rate,  $h$ , is defined as

$$h = k_2 Q_e^2 \quad (13)$$

The values of second-order parameters ' $Q_e$ ,' ' $k_2$ ' and ' $h$ ' are obtained from the linear plot of ' $t/Q_i$ ' versus ' $t$ .' The pseudo-first-order and pseudo-second-order plots are shown in Fig. 11 for all the adsorbates, and the values of both first-order and second-order parameters are listed in Table 2. The adsorption process follows pseudo-second-order model for the adsorption of both the metal ions and the dye since the highest value of regression coefficient ( $R^2$ ) is obtained for this model. The ' $Q_e$ ' value obtained from the calculations is close to the experimental value. Hence, it can be said that the adsorption of the dye and metal ions on Pec-g-poly(AMPS-co-AAm)/Ag follows pseudo-second-order kinetics.

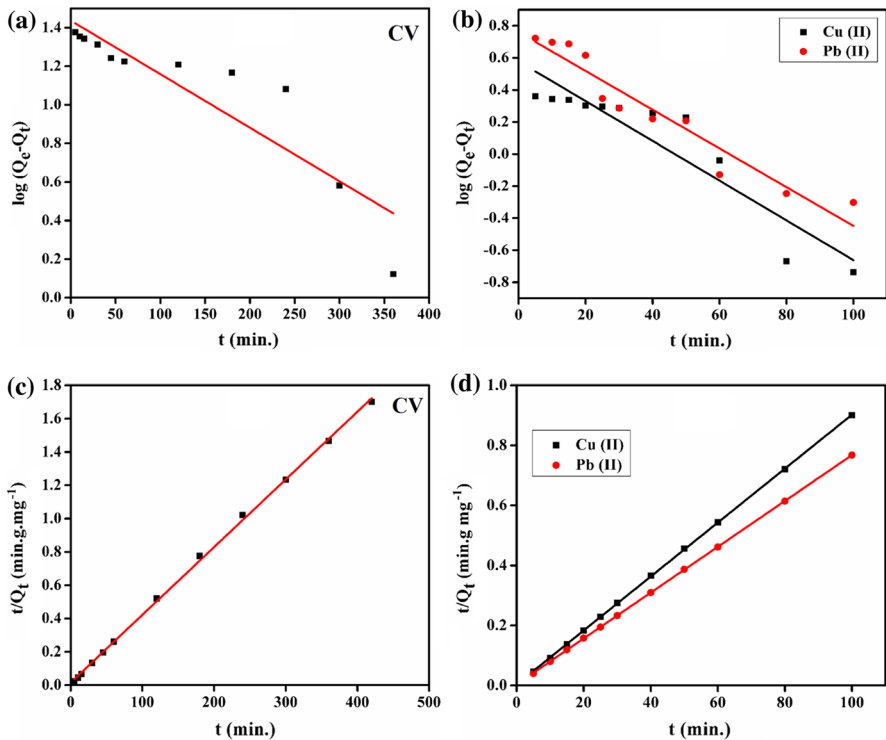


**Fig. 11** a, b Pseudo-first-order plot; c, d pseudo-second-order plot for the adsorption of CV, Cu(II) and Pb(II) on Pec-g-poly(AMPS-co-AAm)/Ag



**Table 2** Kinetic parameters for the adsorption of CV, Cu(II) and Pb(II) on Pec-g-poly(AMPS-co-AAm)/Ag

	Adsorbate		
	CV	Cu(II)	Pb(II)
Concentration ( $C_0$ ) (mg/L)	100	100	100
$Q_e$ , (experimental) (mg/g)	246.8	111.2	130.7
Kinetic model			
Pseudo-first order			
$Q_e$ (mg/g)	27.4	3.8	5.8
$k_1$ ( $\text{min}^{-1}$ )	0.006	0.029	0.028
$R^2$	0.562	0.855	0.927
Pseudo-second order			
$Q_e$ (mg/g)	245.9	111	131
$k_2$ (g/mg/min)	0.001	0.020	0.014
$h$ (mg/g/min)	64.6	252.6	247.1
$R^2$	0.999	1	1

**Thermodynamic parameters** The thermodynamic parameters such as changes in standard free energy ( $\Delta G^\circ$ ), enthalpy ( $\Delta H^\circ$ ) and entropy ( $\Delta S^\circ$ ) associated with adsorption process were calculated from the following equations:

$$\Delta G^\circ = -RT \ln K_c \tag{14}$$

$$\Delta G^\circ = \Delta H^\circ - T\Delta S^\circ \tag{15}$$

where  $K_c$  is the equilibrium constant of adsorption which is obtained from the equation

$$K_c = \frac{Q_e}{C_e} \tag{16}$$

The combination of Eqs. (14) and (15) gives the van't Hoff equation, which is written as

$$\ln K_c = \frac{-\Delta H^\circ}{R} \frac{1}{T} + \frac{\Delta S^\circ}{R} \tag{17}$$

$\Delta H^\circ$  and  $\Delta S^\circ$  were calculated from the slope and intercept of the plot of  $\ln K_c$  versus  $1/T$  (Fig. 12). The values of  $\Delta G^\circ$ ,  $\Delta H^\circ$  and  $\Delta S^\circ$  obtained are listed in Table 3. The negative value of  $\Delta S^\circ$  indicates an ordered arrangement of adsorbate during the adsorption process.  $\Delta H^\circ$  value obtained is negative, and it suggests the adsorption process to be exothermic in nature. The adsorption process can be considered as spontaneous in all cases as the  $\Delta G^\circ$  values obtained are negative.

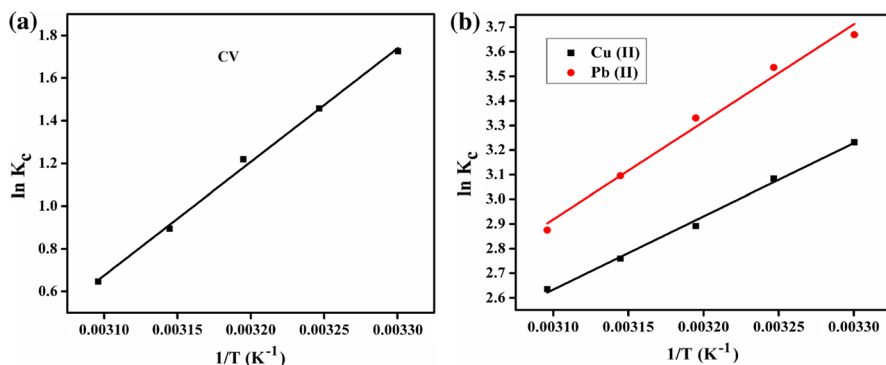


**Fig. 12** Plot of  $\ln K_c$  versus  $1/T$  to calculate the thermodynamic parameters for the adsorption of CV, Cu(II) and Pb(II) on Pec-*g*-poly(AMPS-*co*-AAm)/Ag

**Table 3** Thermodynamics parameters for the adsorption of CV, Cu(II) and Pb(II) on Pec-*g*-poly(AMPS-*co*-AAm)/Ag

Adsorbate	$-\Delta H^\circ$ (kJ/mol)	$-\Delta S^\circ$ (kJ/mol/K)	$-\Delta G^\circ$ (kJ/mol)				
			303 K	308 K	313 K	318 K	323 K
CV	44.25	0.13	4.35	3.73	3.17	2.36	1.74
Cu(II)	24.73	0.05	8.14	7.90	7.53	7.30	7.08
Pb(II)	32.98	0.08	9.24	9.06	8.67	8.18	7.79

## Desorption study

The possibility and extent of desorption of metal ions [Cu(II) and Pb(II)] and dye molecules (CV) from the metal ion- and dye-loaded samples were studied. Aqueous solution of pH 1.2 (prepared using HCl solution) was used as the stripping solution. At acidic pH, the carboxylic groups of pectin and sulfate group of PAMPS get protonated due to their high affinity for acidic protons, resulting in a weak interaction with the metal ions and the dye. The metal ions and dye thus get released to the aqueous medium. The results of adsorption and desorption experiments are shown in Fig. 13. About 97% CV, 99% Cu (II) and 99% Pb(II) adsorbed by the gel are observed to be released in the first desorption cycle.

## Leaching of AgNPs

The percentage of AgNPs leached, when the nanocomposite was kept immersed in double distilled water, is shown in Fig. 14. The number of nanoparticles desorbed from the gel increases with time initially and tends to saturate after 24 h. Even at saturation, only 12% of the total particles incorporated are found to

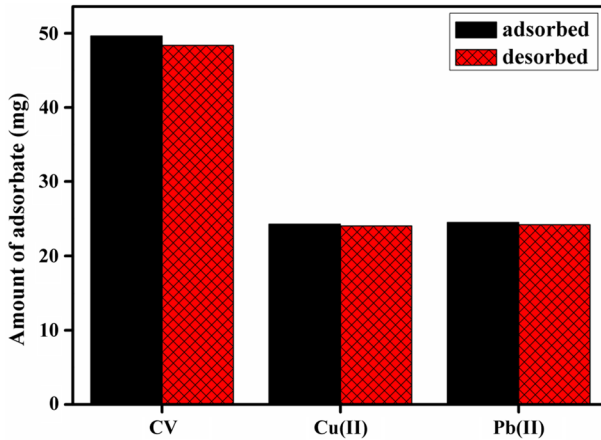
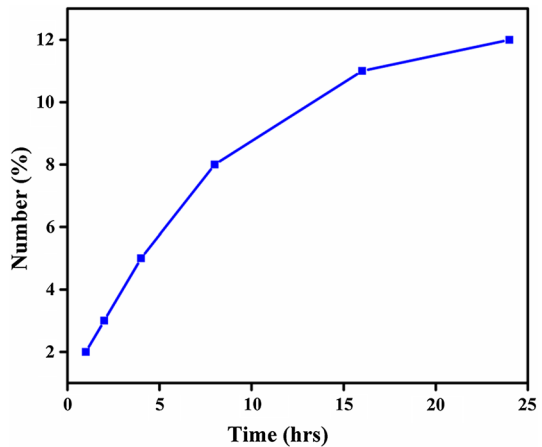


**Fig. 13** Amount of adsorbate adsorbed from aqueous solution and desorbed to stripping solution of pH 1.2

**Fig. 14** Extent of diffusion of AgNPs from Pec-*g*-poly(AMPS-*co*-AAm)/Ag in water



diffuse out. This indicates that the Ag particles are held tight by the polymer network.

**Comparison of the adsorption efficiency of the nanocomposite hydrogel with other adsorbents**

A comparison of the adsorption capacity of the presently studied nanocomposite hydrogel Pec-*g*-poly(AMPS-*co*-AAm)/Ag with other polymeric materials reported in the literature has been made and is presented in Table 4. Few systems among them have been used for the adsorption of both cationic dyes and divalent metal ions. Many polymeric systems [18, 44–49] have been reported for the adsorptive removal of crystal violet from aqueous solutions. But the

**Table 4** Comparative study of adsorption capacity of Pec-*g*-poly(AMPS-*co*-AAm)/Ag with other adsorbents

Adsorbent	$Q_e$ (mg/g)		
	CV	Cu(II)	Pb(II)
Silsesquioxane–TPE polymers [44]	862		
HPMC- <i>g</i> -PAAm/Na-MMt (Clay 12.7) [48]	29.5		
PAAm–Kaolin [2]	23.8		
Magnetite/pectin [18]	140.49		
Chitosan magnetic microspheres (CS-MCM) [47]	82.2		
Glutamic acid-modified CS-MCM [47]	390		
Fe <sub>3</sub> O <sub>4</sub> -coated biochar [49]	289.91		
PANI nanoparticles [46]	0.589		
Carboxymethyl starch- <i>g</i> -PVI magnetic beads [45]	91.58	83.60	65
Chitosan-poly(acrylic acid)-graphene oxide beads [50]			138.89
Thiacalix [4] arenetetrasulfonate-reduced graphene oxide [51]			230
Disulfide-grafted polyethyleneimine-Mg <sub>2</sub> SiO <sub>4</sub> [52]			400
Palm shell-activated carbon [54]		1.581	1.337
Pectin/PAAm semi-IPN hydrogel [53]		203.7	
Tetraethylenepentamine- maleopimaric acid anhydride micelle [57]		761.25	
nPMMA <sub>U5</sub> core-shell particles [55]		80	86
Silica-bipyridine framework [56]		64.84	99.68
P-PAMPS-PAAm/ZnO [34]		77	125
(GG- <i>g</i> -PAAm)-PVA [24]	45.15		
Pec- <i>g</i> -poly(AMPS- <i>co</i> -AAm)/Ag [this work]	1950	111	130

nanocomposite material reported in the present study exhibits the highest adsorption capacity which is 1950 mg/g. Recently, Saad et al. [46] have reported the synthesis of polyaniline nanoparticles and their use for the adsorption of CV through ultrasonicated adsorption process by which 0.589 mg/g of CV was removed. A maximum of 862 mg/g CV adsorption has been achieved with the use of silsesquioxane-based tetraphenylethene-linked nanoporous polymers, a multifunctional hybrid fluorescent porous material [44] with high surface area. The glutamic acid-modified chitosan magnetic composite microspheres [47] showed a maximum adsorption of 390 mg/g. Even the pectin/magnetite hybrid nanocomposite [18] showed less adsorptive removal in comparison with the present study. Magnetic hydrogel beads based on poly(vinyl alcohol)/carboxymethyl starch-*g*-poly(vinyl imidazole) [45] have been used for the adsorptive removal of both the metal ions and the cationic dyes and show moderate efficiency. When compared to other systems such as graphene oxide-incorporated chitosan-poly(acrylic acid) porous polymer nanocomposite [50], thiacalix [4] arenetetrasulfonate-functionalized reduced graphene oxide [51], organically modified magnesium silicate nanocomposite [52] and pectin/poly(acrylamide-*co*-acrylamidoglycolic acid) pH-sensitive semi-IPN hydrogel [53], Pec-*g*-poly(AMPS-*co*-AAm)/Ag showed a

low level adsorption of Cu(II) and Pb(II) ions. Palm shell-activated carbon [54], poly(methyl methacrylate) core–surfactin shell nanoparticles [55] and covalently modified of highly chelated hybrid material based on silica-bipyridine framework [56], etc., showed less adsorption of the metal ions in comparison with adsorbent systems reported in our previous [34] and present works.

## Conclusions

In the present study, a nanocomposite system, Pec-*g*-poly(AMPS-*co*-AAm)/Ag, has been made under microwave irradiation and characterized. The system was tested for its capacity to adsorb a cationic dye, CV and divalent metal ions: Cu(II) and Pb(II) from aqueous solutions at different temperatures. Kinetic, isothermal and thermodynamic studies of the adsorption process have been carried out for each adsorbate, and the corresponding parameters have been reported. The adsorption of CV, Cu(II) and Pb(II) on the nanocomposite hydrogel followed second-order kinetics and fits well with Langmuir isotherm model. Thermodynamic studies revealed that the adsorption process is endothermic and spontaneous at the studied temperatures. The nanocomposite hydrogel was found to remove 1950 mg/g CV, 111 mg/g Cu(II) and 130 mg/g Pb(II) from the aqueous solutions. Reusability of the nanocomposite system was tested by desorption studies, and it was found that the system was able to desorb 97% CV, 99% Cu(II) and Pb(II) to a stripping solution of pH 1.2. The results of the study indicate that the material, Pec-*g*-poly(AMPS-*co*-AAm)/Ag, may in the future be a promising material for the adsorptive removal of toxic organic dyestuffs and heavy metal ions from aqueous solutions.

## References

1. Lakshmiopathy R, Sarada NC (2015) A fixed bed column study for the removal of Pb<sup>2+</sup> ions by watermelon rind. *Environ Sci Water Res Technol* 1:244–250. <https://doi.org/10.1039/C4EW00027G>
2. Shirsath SR, Patil AP, Bhanvase BA, Sonawane SH (2015) Ultrasonically prepared poly(acrylamide)-kaolin composite hydrogel for removal of crystal violet dye from wastewater. *J Environ Chem Eng* 3:1152–1162. <https://doi.org/10.1016/j.jece.2015.04.016>
3. Cao J, Cao H, Zhu Y, Wang S, Qian D, Chen G, Sun M, Huang W (2017) Rapid and effective removal of Cu<sup>2+</sup> from aqueous solution using novel chitosan and laponite-based nanocomposite as adsorbent. *Polymers* 9:1–14. <https://doi.org/10.3390/polym9010005>
4. Panic VV, Seslija SI, Nestic AR, Velickovic SJ (2013) Adsorption of azo dyes on polymer materials. *Hem Ind* 67:881–900
5. Salehi R, Arami M, Mahmoodi NM, Bahrami H, Khorramfar S (2010) Novel biocompatible composite (chitosan-zinc oxide nanoparticle): preparation, characterization and dye adsorption properties. *Colloids Surf B* 80:86–93. <https://doi.org/10.1016/j.colsurfb.2010.05.039>
6. Shenvi SS, Isloor AM, Ismail AF, Shilton SJ, Ahmed AA (2015) Humic acid based biopolymeric membrane for effective removal of methylene blue and rhodamine B. *Ind Eng Chem Res* 54:4965–4975. <https://doi.org/10.1021/acs.iecr.5b00761>
7. Mallampati R, Xuanjun L, Adin A, Valiyaveettil S (2015) Fruit peels as efficient renewable adsorbents for removal of dissolved heavy metals and dyes from water. *ACS Sustain Chem Eng* 3:1117–1124. <https://doi.org/10.1021/acssuschemeng.5b00207>

8. Mohammadi AA, Alinejad A, Kamarehie B, Javan S, Ghaderpoury A, Ahmadpour M, Ghaderpoori M (2017) Metal-organic framework Uio-66 for adsorption of methylene blue dye from aqueous solutions. *Int J Environ Sci Technol* 14:1959–1968. <https://doi.org/10.1007/s1376>
9. Pourjavadi A, Hosseini SH, Seidib F, Soleyman R (2013) Magnetic removal of crystal violet from aqueous solutions using polysaccharide-based magnetic nanocomposite hydrogels. *Polym Int* 62:1038–1044. <https://doi.org/10.1002/pi.4389>
10. Wang J, Liu F (2014) Enhanced and selective adsorption of heavy metal ions on ion-imprinted simultaneous interpenetrating network hydrogels. *Des Monomers Polym* 17:19–254. <https://doi.org/10.1080/15685551.2013.771314>
11. Bhattacharyya R, Ray SK (2013) Kinetic and equilibrium modeling for adsorption of textile dyes in aqueous solutions by carboxymethyl cellulose/poly(acrylamide-co-hydroxyethyl methacrylate) semi-interpenetrating network hydrogel. *Polym Eng Sci* 53:2439–2453. <https://doi.org/10.1002/pen.23501>
12. Zhang J, Wang A (2014) Polysaccharide-based composite hydrogels for removal of pollutants from water. CRC Press, Boca Raton
13. Nicolaus B, Moriello VS, Lama L, Poli A, Gambacorta A (2004) Polysaccharides from extremophilic microorganisms. *Orig Life Evol Biosph* 34:159–169
14. Kopecek J (2002) Polymer chemistry: swell gels. *Nature* 417:388–391
15. Ullah F, Othman MBH, Javed F, Ahmad Z, Akil HM (2015) Classification, processing and application of hydrogels: a review. *Mater Sci Eng C* 57:414–433. <https://doi.org/10.1016/j.msec.2015.07.053>
16. Chirani N, Yahia L, Gritsch L, Motta FL, Chirani S, Fare S (2016) History and applications of hydrogels. *J Biomed Sci* 4:1–23. <https://doi.org/10.4172/2254-609X.100013>
17. Tu H, Yu Y, Chen J, Shi X, Zhou J, Deng H, Du Y (2017) Highly cost-effective and high-strength hydrogels as dye adsorbents from natural polymers: chitosan and cellulose. *Polym Chem* 8:2913–2921. <https://doi.org/10.1039/C7PY00223H>
18. Attallah OA, Al-Ghobashy MA, Nebsen M, Salem MY (2016) Removal of cationic and anionic dyes from aqueous solution with magnetite/pectin and magnetite/silica/pectin hybrid nanocomposites: kinetic, isotherm and mechanism analysis. *RSC Adv* 6:11461–11480. <https://doi.org/10.1039/C5RA23452B>
19. Pandey N, Shukla SK, Singh NB (2017) Water purification by polymer nanocomposites: an overview. *Nanocomposites* 3:47–66. <https://doi.org/10.1080/20550324.2017.1329983>
20. Kono H (2015) Preparation and characterization of amphoteric cellulose hydrogels as adsorbents for the anionic dyes in aqueous solutions. *Gels* 1:94–116. <https://doi.org/10.3390/gels1010094>
21. Karthika JS, Vishalakshi B (2015) Novel stimuli responsive gellan gum-graft-poly(DMAEMA) hydrogel as adsorbent for anionic dye. *Int J Biol Macromol* 81:648–655. <https://doi.org/10.1016/j.ijbiomac.2015.08.064>
22. Peng N, Hu D, Zeng J, Li Y, Liang L, Chang C (2016) Superabsorbent cellulose-clay nanocomposite hydrogels for highly efficient removal of dye in water. *ACS Sustain Chem Eng* 4:7217–7224. <https://doi.org/10.1021/acssuschemeng.6b02178>
23. Ghorai S, Sarkar A, Raoufi M, Panda AB, Hchönherr H (2014) Enhanced removal of methylene blue and methyl violet dyes from aqueous solution using a nanocomposite of hydrolyzed polyacrylamide grafted xanthan gum and incorporated nanosilica. *ACS Appl Mater Interfaces* 6:4766–4777. <https://doi.org/10.1021/am4055657>
24. Krishna KA, Vishalakshi B (2017) Gellan gum based novel composite hydrogel: evaluation as adsorbent for cationic dyes. *J Appl Polym Sci* 134:45527–45535. <https://doi.org/10.1002/app.45527>
25. Kurita O, Fujiwara T, Yamazaki E (2008) Characterization of the pectin extracted from citrus peel in the presence of citric acid. *Carbohydr Polym* 74:725–730. <https://doi.org/10.1016/j.carbpol.2008.04.033>
26. Singha NR, Mahapatra M, Karmakar M, Mondal H, Dutta A, Deb M, Mitra M, Roy C, Chattopadhyay PK, Maiti DK (2018) In situ allocation of a monomer in pectin-g-terpolymer hydrogels and effect of comonomer compositions on superadsorption of metal ions/dyes. *ACS Omega* 3:4163–4180. <https://doi.org/10.1021/acsomega.8b00446>
27. Jung J, Arnold RD, Wicker L (2013) Pectin and charge modified pectin hydrogel beads as a colon-targeted drug delivery carrier. *Colloids Surf B Biointerfaces* 104:116–121. <https://doi.org/10.1016/j.colsurfb.2012.11.042>

28. Munarin F, Guerreiro SG, Grellier MA, Tanzi MC, Barbosa MA, Petrini P, Granja PL (2011) Pectin-based injectable biomaterials for bone tissue engineering. *Biomacromolecules* 12:568–577. <https://doi.org/10.1021/bm101110x>
29. Thakur BR, Singh RK, Handa AK, Rao MA (1997) Chemistry and uses of pectin—a review. *Crit Rev Food Sci Nutr* 37:47–73. <https://doi.org/10.1080/10408399709527767>
30. Mishra RK, Datt M, Banthia AK (2008) Synthesis and characterization of pectin/PVP hydrogel membranes for drug delivery system. *AAPS Pharmscitech* 9:395–403. <https://doi.org/10.1208/s12249-008-9048-6>
31. Amin MT, Alazba AA, Manzoor U (2014) A review of removal of pollutants from water/wastewater using different types of nanomaterials. *Adv Mater Sci Eng*. <https://doi.org/10.1155/2014/825910>
32. Basu S, Samanta HS, Ganguly J (2018) Green synthesis and swelling behavior of Ag–nanocomposite semi-IPN hydrogels and their drug delivery using *dolichos biflorus* Lin. *Soft Matter* 16:7–19. <https://doi.org/10.1080/1539445X.2017.1368559>
33. Navarro MAG, Rosales JAA, Vazquez EEL, Cortez IEM, Castro AT, Gonzalez VG (2013) Totally ecofriendly synthesis of silver nanoparticles from aqueous dissolution of polysaccharides. *Int J Polym Sci*. <https://doi.org/10.1155/2013/436021>
34. Krishna KA, Vishalakshi B (2017) Pectin based ZnO nanocomposite hydrogel: evaluation as adsorbent for divalent metal ions from aqueous solutions. *Elixir Nanotechnol* 107:47326–47331
35. Moharana B, Preetha SP, Selvasubramanian S, Malathi S, Balasubramanian S (2014) Synthesis and characterization of pectin capped silver nanoparticles and exploration of its anticancer potentials in experimental carcinogenesis *in vitro*. *Indo Am J Pharm Res* 4:5576–5583. <https://doi.org/10.1044/1980-iajpr.141165>
36. Sundarajan S, Sameem SM, Sankaranarayanan S, Ramaraj S (2013) Synthesis, characterization and application of zero-valent silver nano adsorbents. *IJIRSET* 2:8023–8037
37. Babu VR, Kim C, Kim S, Ahn C, Lee YI (2010) Development of semi-interpenetrating carbohydrate polymeric hydrogels embedded silver nanoparticles and its facile studies on *E. coli*. *Carbohydr Polym* 81:196–202. <https://doi.org/10.1016/j.carbpol.2010.02.050>
38. Kabiri K, Mehr MJZ, Mirzadeh H, Kheirabadi M (2010) Solvent-, ion- and pH-specific swelling of poly(2-acrylamido-2-methylpropane sulfonic acid) superabsorbing gels. *J Polym Res* 17:203–212. <https://doi.org/10.1007/s10965-009-9306-7>
39. Bajpai SK (2001) Swelling-deswelling behavior of poly(acrylamide-co-maleic acid) hydrogels. *J Appl Polym Sci* 80:2782–2789. <https://doi.org/10.1002/app.1394>
40. Gueu S, Yao B, Adouby K, Ado G (2007) Kinetics and thermodynamics study of lead adsorption on to activated carbons from coconut and seed hull of the palm tree. *Int J Environ Sci Technol* 4:11–17. <https://doi.org/10.1007/BF03325956>
41. Langmuir I (1918) The adsorption of gases on plane surfaces of glass, mica and platinum. *J Am Chem Soc* 40:1361–1403. <https://doi.org/10.1021/ja02242a004>
42. Dada AO, Olalekan AP, Olatunya AM, Dada O (2012) Langmuir, Freundlich, Temkin and Dubinin-Radushkevich isotherm studies of equilibrium sorption of  $Zn^{2+}$  unto phosphoric acid modified rice husk. *IOSR-JAC* 3:38–45. <https://doi.org/10.9790/5736-0313845>
43. Ho YS, McKay G (1999) Pseudo-second order model for sorption process. *Process Biochem* 34:451–465. [https://doi.org/10.1016/S0032-9592\(98\)00112-5](https://doi.org/10.1016/S0032-9592(98)00112-5)
44. Liu H, Liu H (2017) Selective dye adsorption and metal ion detection using multifunctional silsesquioxane-based tetraphenylethene-linked nanoporous polymers. *J Mater Chem A* 5:9156–9162. <https://doi.org/10.1039/C7TA01255A>
45. Pour ZS, Ghaemy M (2015) Removal of dyes and heavy metal ions from water by magnetic hydrogel beads based on poly(vinyl alcohol)/carboxymethyl starch-g-poly(vinyl imidazole). *RSC Adv* 5:64106–64118. <https://doi.org/10.1039/C5RA08025H>
46. Saad M, Tahir H, Khan J, Hameed U, Saud A (2017) Synthesis of polyaniline nanoparticles and their application for the removal of Crystal Violet dye by ultrasonicated adsorption process based on response surface methodology. *Ultrason Sonochem* 34:600–608. <https://doi.org/10.1016/j.ultsonch.2016.06.022>
47. Yan H, Li H, Yang H, Li A, Cheng R (2013) Removal of various cationic dyes from aqueous solutions using a kind of fully biodegradable magnetic composite microsphere. *Chem Eng J* 223:402–411. <https://doi.org/10.1016/j.cej.2013.02.113>
48. Mahdavinia GR, Hasanpour J, Rahmani Z, Karami S, Etemadi H (2013) Nanocomposite hydrogel from grafting of acrylamide onto HPMC using sodium montmorillonite nanoclay and removal of crystal violet dye. *Cellulose* 20:2591–2604. <https://doi.org/10.1007/s10570-013-0004-6>

49. Sun P, Hui C, Khan RA, Du J, Zhang Q, Zhao YH (2015) Efficient removal of crystal violet using Fe<sub>3</sub>O<sub>4</sub>-coated biochar: the role of the Fe<sub>3</sub>O<sub>4</sub> nanoparticles and modeling study their adsorption behavior. *Sci Rep* 5:1–15. <https://doi.org/10.1038/srep12638>
50. Medina RP, Nadres ET Jr, Florencio CB, Rodrigues DF (2016) Incorporation of graphene oxide into chitosan-poly(acrylic acid) porous polymer nanocomposite for enhanced lead adsorption. *Environ Sci Nano* 3:638–646. <https://doi.org/10.1039/C6EN00021E>
51. Liu C, Zhang D, Zhao L, Lu X, Zhang P, He S, Hu G, Tang X (2016) Synthesis of a thiacalix[4]arenetetrasulfonatefunctionalized reduced graphene oxide adsorbent for the removal of lead(II) and cadmium(II) from aqueous solutions. *RSC Adv* 6:113352–113365. <https://doi.org/10.1039/C6RA24353C>
52. Yu Y, Hu Z, Chen Z, Yang J, Gao H, Chen Z (2016) Organically-modified magnesium silicate nanocomposites for high-performance heavy metal removal. *RSC Adv* 6:97523–97531. <https://doi.org/10.1039/C6RA20181D>
53. Reddy NS, Rao KM, Vania TJS, Rao KSVK, Lee YI (2015) Pectin/poly(acrylamide-co-acrylamidoglycolic acid) pH sensitive semi-IPN hydrogels: selective removal of Cu<sup>2+</sup> and Ni<sup>2+</sup>, modeling, and kinetic studies. *Desalin Water Treat* 57:6503–6514. <https://doi.org/10.1080/19443994.2015.1008053>
54. Onundi YB, Mamun AA, Al Khatib MF, Ahmed YM (2010) Adsorption of copper, nickel and lead ions from synthetic semiconductor industrial wastewater by palm shell activated carbon. *Int J Environ Sci Technol* 7:751–758. <https://doi.org/10.1007/BF03326184>
55. Kundu D, Hazra C, Chatterjee A, Chaudhari A, Mishra S (2014) Sonochemical synthesis of poly(methyl methacrylate) core-surfactin shell nanoparticles for recyclable removal of heavy metal ions and its cytotoxicity. *RSC Adv* 4:24991–25004. <https://doi.org/10.1039/C4RA03008G>
56. Radi S, Tighadouini S, Bacquet M, Degoutin S, Janus L, Mabkhot YN (2016) Fabrication and covalent modification of highly chelate hybrid material based on silica-bipyridine framework for efficient adsorption of heavy metals: isotherms, kinetics and thermodynamics studies. *RSC Adv* 6:82505–82514. <https://doi.org/10.1039/C6RA14349K>
57. Tan WX, Lin ZT, Bu HT, Tian Y, Jiang GB (2012) Nano-micelles based on a rosin derivative as potent sorbents and sinking agents with high absorption capabilities for the removal of metal ions. *RSC Adv* 2:7279–7289. <https://doi.org/10.1039/C2RA20767B>

**Publisher's Note** Springer Nature remains neutral with regard to jurisdictional claims in published maps and institutional affiliations.